The 2175 Å Extinction Feature in the Optical Afterglow Spectrum of GRB 180325A at $z = 2.25$[*]

T. Zafar[1] , K. E. Heintz[2,3], J. P. U. Fynbo[3] , D. Malesani[4] , J. Bolmer[5], C. Ledoux[5], M. Arabsalmani[6], L. Kaper[7], S. Campana[8], R. L. C. Starling[9], J. Selsing[4] , D. A. Kann[10], A. de Ugarte Postigo[4,10], T. Schweyer[11,12], L. Christensen[4] , P. Møller[13] , J. Japelj[7], D. Perley[14] , N. R. Tanvir[9] , P. D'Avanzo[15], D. H. Hartmann[16] , J. Hjorth[4], S. Covino[17] , B. Sbarufatti[18], P. Jakobsson[2], L. Izzo[10] , R. Salvaterra[19] , V. D'Elia[20,21], and D. Xu[22]

[1] Australian Astronomical Observatory, PO Box 915, North Ryde, NSW 1670, Australia; tayyaba.zafar@aao.gov.au
[2] Centre for Astrophysics and Cosmology, Science Institute, University of Iceland, Dunhagi 5, 107 Reykjavík, Iceland
[3] The Cosmic Dawn Center, Niels Bohr Institute, University of Copenhagen, Juliane Maries Vej 30, DK-2100 Copenhagen Ø, Denmark
[4] Dark Cosmology Centre, Niels Bohr Institute, University of Copenhagen, Juliane Maries Vej 30, DK-2100 Copenhagen Ø, Denmark
[5] European Southern Observatory, Alonso de Córdova 3107, Vitacura, Casilla 19001, Santiago de Chile, Chile
[6] Université Paris Diderot, AIM, Sorbonne Paris Cité, CEA, CNRS, F-91191 Gif-sur-Yvette, France
[7] Astronomical Institute Anton Pannekoek, University of Amsterdam, Science Park 904, 1098 XH, Amsterdam, the Netherlands
[8] INAF—Osservatorio astronomico di Brera, Via E. Bianchi 46, Merate (LC) I-23807, Italy
[9] Department of Physics and Astronomy, University of Leicester, University Road, Leicester LE1 7RH, UK
[10] Instituto de Astrofísica de Andalucía (IAA-CSIC), Glorieta de la Astronomía, s/n, E-18008 Granada, Spain
[11] Max-Planck Institut für Extraterrestrische Physik, Giessenbachstr. 1, D-85748 Garching, Germany
[12] Technische Universität München, Physik Department, James-Franck-Str., D-85748 Garching, Germany
[13] European Southern Observatory, Karl-Schwarzschild-Strasse 2, D-85748, Garching, Germany
[14] Astrophysics Research Institute, Liverpool John Moores University, 146 Brownlow Hill, IC2 Liverpool Science Park, Liverpool L3 5RF, UK
[15] INAF-Osservatorio Astronomico di Brera, Via Bianchi 46, I-23807, Merate (LC), Italy
[16] Department of Physics and Astronomy, Clemson University, Clemson, SV 29634-0978, USA
[17] INAF/Brera Astronomical Observatory, Via Bianchi 46, I-23807, Merate (LC), Italy
[18] Department of Astronomy and Astrophysics, The Pennsylvania State University, 525 Davey Lab, University Park, PA 16802, USA
[19] INAF—IASF/Milano, via Bassini 15, I-20133 Milano, Italy
[20] Space Science Data Center—Agenzia Spaziale Italiana, via del Politecnico, s.n.c., I-00133, Roma, Italy
[21] INAF—Astronomical Observatory of Rome, via Frascati 33, Monte Porzio Catone I-00040, Roma, Italy
[22] National Astronomical Observatories, Chinese Academy of Sciences, Beijing 100012, People's Republic of China

Abstract

The ultraviolet (UV) extinction feature at 2175 Å is ubiquitously observed in the Galaxy but is rarely detected at high redshifts. Here we report the spectroscopic detection of the 2175 Å bump on the sightline to the γ-ray burst (GRB) afterglow GRB 180325A at $z = 2.2486$, the only unambiguous detection over the past 10 years of GRB follow-up, at four different epochs with the Nordic Optical Telescope (NOT) and the Very Large Telescope (VLT)/X-shooter. Additional photometric observations of the afterglow are obtained with the Gamma-Ray burst Optical and Near-Infrared Detector (GROND). We construct the near-infrared to X-ray spectral energy distributions (SEDs) at four spectroscopic epochs. The SEDs are well described by a single power law and an extinction law with $R_V \approx 4.4$, $A_V \approx 1.5$, and the 2175 Å extinction feature. The bump strength and extinction curve are shallower than the average Galactic extinction curve. We determine a metallicity of $[\mathrm{Zn/H}] > -0.98$ from the VLT/X-shooter spectrum. We detect strong neutral carbon associated with the GRB with equivalent width of $W_r(\lambda\,1656) = 0.85 \pm 0.05$. We also detect optical emission lines from the host galaxy. Based on the Hα emission-line flux, the derived dust-corrected star formation rate is $\sim 46 \pm 4\ M_\odot\,\mathrm{yr}^{-1}$ and the predicted stellar mass is $\log M_*/M_\odot \sim 9.3 \pm 0.4$, suggesting that the host galaxy is among the main-sequence star-forming galaxies.

Key words: dust, extinction – galaxies: ISM – gamma-ray burst: general – gamma-ray burst: individual (GRB 180325A)

Supporting material: machine-readable table

1. Introduction

Dust plays an important role in the formation and evolution of galaxies. Extinction curves as a function of wavelength provide information on dust grain sizes and compositions (Draine 2003). Long-duration γ-ray bursts (GRBs) are powerful probes to study absolute extinction curves of distant star-forming galaxies because of their bright afterglow emission, simple spectral shape (Sari et al. 1998), association with short-lived massive stars (e.g., Cano et al. 2017), and location in star-forming regions (e.g., Fynbo et al. 2000; Starling et al. 2011). Broadband spectroscopy of GRB afterglows allows us to study individual line-of-sight absolute extinction curves (Zafar et al. 2011, 2018), and provides information about chemical abundances (Cucchiara et al. 2015) and gas kinematics (Arabsalmani et al. 2015) in their host galaxies.

A characteristic feature in the Milky Way (MW) extinction curve is an absorption bump centered at 2175 Å, first discovered by Stecher (1965). The feature is ubiquitously seen in MW extinction curves (Fitzpatrick & Massa 2007). The bump strength drops in the interstellar extinction curves of the Large Magellanic Cloud (LMC; Gordon et al. 2003) and is only seen in a few sightlines toward the Small Magellanic Cloud (SMC; Gordon et al. 2003; Maíz Apellániz & Rubio 2012). The exact origin of the feature is still unclear, although some candidates, such as non-graphitic carbon (Mathis 1994) or polycyclic aromatic hydrocarbons (Draine 2003), have been proposed. The reduction in extinction bump strength for different environments is attributed to low metallicities (Fitzpatrick 2004) or different radiative environments (Mattsson et al. 2008).

Beyond the local universe, the 2175 Å extinction feature becomes very uncommon (e.g., Zeimann et al. 2015; Reddy et al. 2018). At $z > 1$, the extinction bump has been detected in the Great Observatories Origins Deep Survey (GOODS)-*Herschel* field galaxies (Buat et al. 2011). A sample of massive star-forming galaxies at $z \sim 2$ shows 2175 Å bumps in their spectra (Noll et al. 2007). Weaker bumps for active galaxies have been found from the spectral energy distributions (SEDs) of $0.5 < z < 2.0$ galaxies (Kriek & Conroy 2013). In a sample of $2 \leqslant z \leqslant 6.5$ COSMOS galaxies, a 2175 Å bump is reported based on photometry (Scoville et al. 2015). The extinction feature is also detected in several metal-line absorbing systems toward quasar sightlines (e.g., Jiang et al. 2011; Ma et al. 2018). In GRBs, a significant spectroscopic 2175 Å bump has been confirmed only in four GRBs (GRB 070802: Krühler et al. 2008; Elíasdóttir et al. 2009, GRB 080607: Prochaska et al. 2009; Perley et al. 2011, GRB 080605 and GRB 080805: Zafar et al. 2012). The peculiar extinction curve toward GRB 140506A does not seem to be caused by an extreme version of the 2175 Å extinction feature, but rather by a different phenomenon, the nature of which remains unknown (Fynbo et al. 2014; Heintz et al. 2017). In general, by studying a γ-ray flux limited sample, Covino et al. (2013) found that the 2175 Å feature is required in at least 15% of cases to account for the broadband photometric afterglow SED.

Here, we report another significant *spectroscopic* detection of a 2175 Å bump, discovered in the optical spectrum of GRB 180325A, nearly a decade since the last reported unambiguous examples. This dearth is despite the powerful current generation of instruments, in particular, the Very Large Telescope (VLT)/X-shooter (Vernet et al. 2011). The VLT/X-shooter enables near-infrared (NIR) to ultraviolet (UV) observations in one shot and is ideally suited to discover such a feature. This Letter is organized as follows. In Section 2 we describe multi-wavelength observations of the GRB 180325A afterglow carried out with different instruments. In Section 3 we present our SED and optical spectrum analysis results. A discussion is provided in Section 4 and conclusions in Section 5.

2. Observations and SED Construction

At 01:53:02 UT on 2018 March 25, the *Neil Gehrels Swift Observatory* detected GRB 180325A with its Burst Alert Telescope (BAT), and its X-Ray Telescope (XRT) began observations at 01:54:16.2 UT. At 6 minutes after the burst trigger, the Nordic Optical Telescope (NOT) equipped with the Andalucia Faint Object Spectrograph and Camera (AlFOSC) observed the GRB in the R-band. A sequence of 3×600 sec

Table 1
Multiband Photometric Observations of GRB 180325A

Facility-filter-band	Time since Trigger (s)	Exposure Time (s)	Observed Magnitude AB (mag)
NOT-R	568.2	100.0	18.51 ± 0.04
NOT-R	3091.2	100.0	19.23 ± 0.04
GROND-g'	3791.114	184.9	20.24 ± 0.03
GROND-r'	3791.114	184.9	19.32 ± 0.03
GROND-i'	3791.114	184.9	18.95 ± 0.03

(This table is available in its entirety in machine-readable form.)

spectra with a mean time of 2:26 UT using a $1''3$ wide slit and grism 4 (with spectral coverage from 3800 to 9200 Å and resolution $R = \lambda/\Delta\lambda = 277$) were obtained with AlFOSC. A strong 2175 Å bump was immediately obvious (Heintz et al. 2018). Another AlFOSC 2000 s spectrum was taken with grism 20 (with spectral coverage from 6000 to 9200 Å and $R = 560$) using a $1''3$ slit.

The Gamma-Ray burst Optical and Near-Infrared Detector (GROND) mounted at the 2.2 m Max Planck Gesellschaft telescope started taking photometric observations of the afterglow in all seven ($g' r' i' z' JH$ and K) bands at ~ 1.05 hr after the burst. The complete log of GROND, NOT, and VLT/X-shooter photometric observations is provided in Table 1. The AB magnitudes provided in Table 1 are not corrected for Galactic extinction. From the photometry we construct multi-band optical/NIR lightcurves. The temporal behavior of the r'-band lightcurve (between 0.3 and 8.3 hr) follows a broken power law with a break at $t_b = 6.48 \pm 1.20$ ks and decay slopes $\alpha_1 = 0.02 \pm 0.03$ and $\alpha_2 = 2.00 \pm 0.13$ following the convention where $F_\nu \propto \nu^{-\alpha}$. The lightcurves of all other bands follow a consistent behavior.

We subsequently observed GRB 180325A at ~ 1.84 hr after trigger with the VLT/X-shooter spectrograph. VLT/X-shooter data were obtained as part of the Stargate VLT proposal (Program ID: 0100.D−0649(A)) and the spectra were reduced following the approach outlined in Selsing et al. (2018). The VLT/X-shooter spectrograph covers the spectral wavelength range from 3000 to 24800 Å, divided into three spectroscopic arms. The spectroscopic sequence consisted of two epochs of 4×600 s exposure each and were observed following an ABBA nodding pattern. The slits were aligned with the parallactic angle, and used slit widths are $1''0$, $0''9$ and $0''9$ for the UVB, VIS, and NIR arm, respectively. This corresponds to a spectral resolution of 5400 (UVB), 8900 (VIS), and 5600 (NIR). The spectra were taken under good conditions with a median seeing of $1''0$ at 6700 Å and at airmass ranging from 1.52 to 1.75. Throughout this Letter, the wavelengths are reported in vacuum and are shifted to the heliocentric velocity. All optical data were corrected for a Galactic extinction of $E(B - V) = 0.02$ mag using the dust maps of Schlafly & Finkbeiner (2011). As it is only a small correction, the uncertainty due to the Galactic extinction correction is negligible. All four, NOT and VLT/X-shooter, spectra in the extinction bump region are shown in Figure 1. The central redshift obtained from metal lines in the VLT/X-shooter spectrum is $z = 2.2486$ and the derived H I column density is $\log N(\text{H I}/\text{cm}^{-2}) = 22.30 \pm 0.14$ (see Figure 1 inset). The
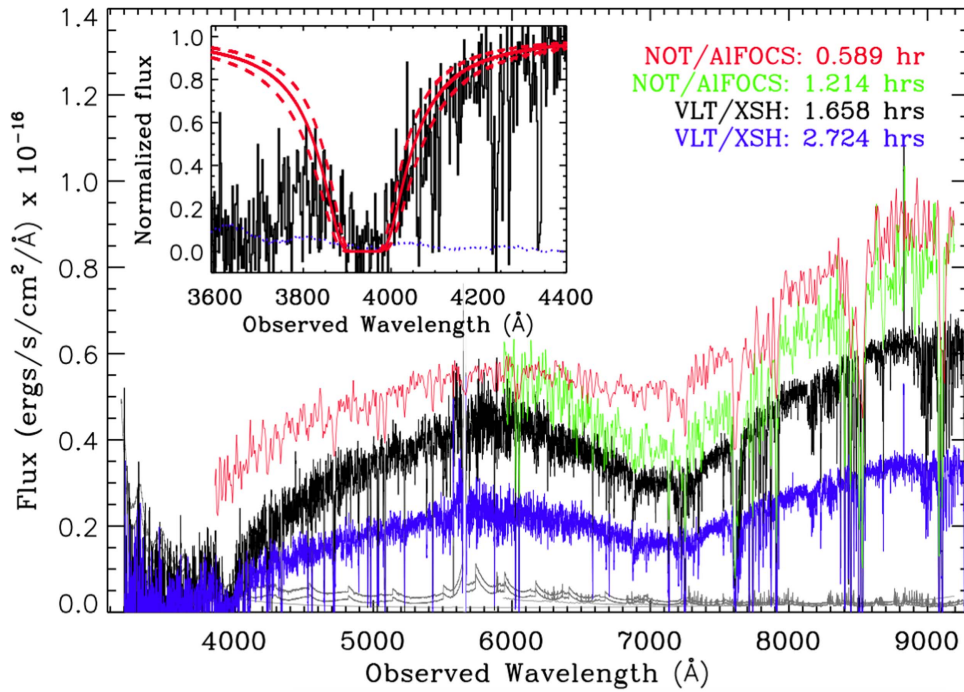
Figure 1. Optical afterglow spectra of GRB 180325A (in the extinction bump region) at four epochs observed with the NOT/AlFOSC and VLT/X-shooter instruments. Each color corresponds to a different epoch and mid-times of observations are indicated in the corresponding color. Inset: shown is the VLT/X-shooter spectrum and corresponding noise spectrum (blue dotted line) in the Lyα absorption-line region. The red solid and dashed lines show the best-fit H I column density profile and 1σ error, respectively.

spectrum also shows the presence of a strong intervening system at $z = 2.04$.

The X-ray spectra and lightcurves were extracted in the 0.3–10 keV range following the method of Evans et al. (2009). The entire XRT photon counting (PC)-mode data set does not show strong spectral variations, thus justifying a fit with a single power law. The best fit is with a photon index $\Gamma = 1.84 \pm 0.10$ and host galaxy equivalent neutral hydrogen column density, $N_{\mathrm{H,X}} = 1.33^{+0.42}_{-0.41} \times 10^{22}$ cm^{-2}, where the Galactic H I column density is set to 1.23×10^{20} cm^{-2} and Galactic molecular H$_2$ column density to 6.27×10^{18} cm^{-2} using the nH tool[23] following the method of Willingale et al. (2013). We construct four XRT spectra around the SED epochs for the SED fitting (see Section 3). These four spectra are normalized to the photometric SED mid-points by considering the photon-weighted mean times and using the lightcurve decay power-law ($\alpha_X = 2.10^{+0.07}_{-0.06}$) fit. The XRT data show no evidence of spectral evolution around the four spectra so the lightcurve hardness-ratio does not deviate from the mean.

3. Results

3.1. SED Fitting and Extinction Curve

We followed the SED fitting method described in Zafar et al. (2018). We used the spectral fitting package XSPEC (v12.9; Arnaud 1996) to fit the multi-epoch restframe NIR to X-ray SEDs of GRB 180325A. The SEDs were modeled with a single or broken power law plus Fitzpatrick & Massa (1990) parametric extinction law and soft X-ray absorption. We refer the reader to Zafar et al. (2018) for a more detailed description of the model. Briefly, the Fitzpatrick & Massa (1990) dust law consists of: (i) a UV linear component given as c_1 (intercept)

and c_2 (slope) with c_4 defining the far-UV curvature and (ii) a Drude component specifying the 2175 Å extinction feature by c_3 (bump strength), x_0 (central wavelength), and γ (bump width) parameters. The *total* Galactic equivalent neutral hydrogen column density ($N_{\mathrm{H,Gal}}$) was fixed to the values obtained from Willingale et al. (2013), 1.29×10^{20} cm^{-2}. The soft X-ray absorption, $N_{\mathrm{H,X}}$, is left as a free parameter and modeled with ztbabs.

Except for the case of GRB 080605 (two epochs; Zafar et al. 2012), the 2175 Å bump for GRB afterglows has not been spectroscopically observed at more than one epoch in any case. We here for the first time spectroscopically observed the extinction bump at four epochs. We used GROND photometric data and lightcurves (only for first epoch) to construct the X-ray to NIR SEDs around all four spectroscopic epochs. The X-ray data and optical spectra are scaled to the photometric mid-points. For X-shooter SEDs, the GROND data is only used for the normalization of spectra where difference is usually <10%. For NOT SEDs, the GROND data outside the spectral coverage is incorporated in the SED fitting. We find that the SEDs at all epochs are fit well with a single power law and a 2175 Å extinction curve (see, however, notes in Table 2). We also tested if the bump is related to the intervening absorber at $z = 2.04$, and find no evidence. The SED and extinction curve at $\Delta t = 1.6314$ hr are shown in Figure 2. The best-fit results of the SEDs are reported in Table 2. We find that for all four epochs, the extinction curve parameters are consistent, particularly the total-to-selective extinction (R_V) and the total extinction at V-band (A_V) are consistent within 1σ.

3.2. Metal Absorption Lines

Through a Lyα Voigt profile fit we derive a column density of $\log N(\mathrm{H\,I/cm}^{-2}) = 22.30 \pm 0.14$ for atomic neutral

---

Table 2
Results of the SED Best-fit Parameters for GRB 180325A X-Ray to NIR SEDs

SED	Δt (hr)	$N_{\rm H,X}$ (10^{22} cm^{-2})	β	c_1 (μm)	c_2	c_3	c_4 (μm^2)	γ (μm^{-1})	x_0 (μm^{-1})	R_V	A_V (mag)	χ^2_ν/dof	NHP%
NOT$-$XRT[a]	0.5833	$0.59^{+0.31}_{-0.29}$	0.76 ± 0.13	-1.92 ± 0.21	1.38 ± 0.16	3.10 ± 0.21	1.20 ± 0.25	1.14 ± 0.03	4.540 ± 0.02	$4.40^{+0.23}_{-0.19}$	$1.63^{+0.12}_{-0.10}$	1.00/881	51
NOT$-$XRT	1.1953	$0.61^{+0.30}_{-0.29}$	0.78 ± 0.12	-2.17 ± 0.27	1.31 ± 0.23	3.34 ± 0.25	1.21 ± 0.47	1.15 ± 0.03	4.540 ± 0.02	$4.38^{+0.21}_{-0.18}$	$1.55^{+0.11}_{-0.09}$	0.96/887	78
XSH$-$XRT	1.6314	$0.70^{+0.22}_{-0.19}$	$0.85^{+0.14}_{-0.13}$	-1.95 ± 0.39	1.28 ± 0.17	2.92 ± 0.19	0.52 ± 0.14	1.16 ± 0.06	4.538 ± 0.03	$4.58^{+0.37}_{-0.39}$	$1.58^{+0.10}_{-0.12}$	0.96/33572	100
XSH$-$XRT	2.9866	$1.20^{+0.37}_{-0.30}$	$0.89^{+0.12}_{-0.10}$	-2.04 ± 0.34	1.26 ± 0.24	3.05 ± 0.22	0.32 ± 0.21	1.13 ± 0.05	4.534 ± 0.03	$4.46^{+0.41}_{-0.37}$	$1.37^{+0.14}_{-0.10}$	0.99/33291	90

Note. The columns give the SED photometric mid-point, the equivalent neutral hydrogen column density, intrinsic slope β, UV linear intercept c_1, UV slope c_2, bump strength c_3, far-UV curvature c_4, bump width γ, bump central wavelength x_0, R_V, visual extinction, reduced χ^2 with number of degrees of freedom (dof) and null hypothesis probability (NHP).
[a] Note that the spectrum and early photometry are affected by the host contribution. The XRT and multiband photometric data are also not available at that time and SED is generated from the lightcurve extrapolation. The lightcurves show signs of evolution, therefore, the results should not be considered reliable.
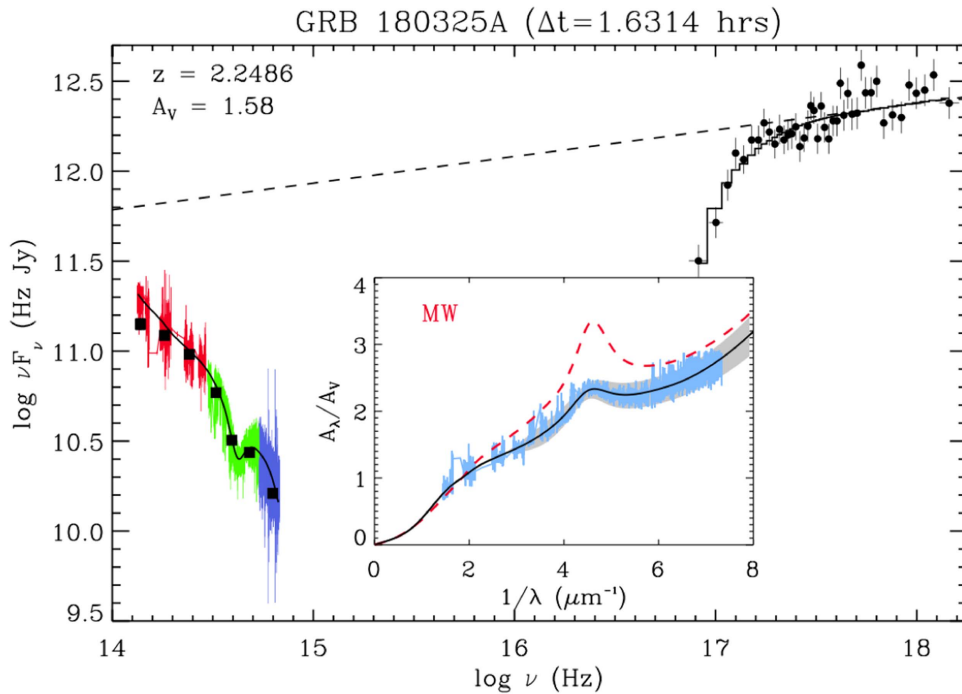
Figure 2. Observer-frame afterglow SED of GRB 180325A. Black circles indicate the *Swift* X-ray data. The binned (for visual purposes) blue, green, and red data points (with 1σ errors) correspond to the UVB, VIS, and NIR VLT/X-shooter spectra, respectively. GROND observations are represented by black squares. The black solid and dashed lines show the best-fit dusty+absorbed and intrinsic spectral model, respectively. Inset: the black line shows the absolute extinction curve, and the gray shaded area materializes the associated 1σ uncertainty. The X-shooter spectra are indicated by cyan curves. The red dashed line corresponds to the mean MW curve from Fitzpatrick & Massa (2007).

hydrogen along the GRB sightline. To measure the gas-phase metallicity of the host galaxy, we fit multi-component Voigt profiles to the low-ionization metal lines in the spectrum using VOIGTFIT (Krogager 2018). We show the best-fit Voigt profiles in Figure 3 to some of these metal lines. The derived column densities and abundances are reported in Table 3, where solar photospheric abundances from Asplund et al. (2009) are assumed. The metal lines are all heavily saturated (except for Cr II and C I), therefore, we report those abundances as lower limits. Note that Cr is depleted onto dust, and therefore its abundance is not an indicator of the true metallicity. Using the column density of Zn, we derive a lower limit of $[\mathrm{Zn/H}] \geqslant -0.98$ for the metallicity of the host galaxy. We also use the low-ionization lines and measure a lower limit of $\Delta v_{90} \leqslant 180$ km s^{-1} for the velocity width of neutral gas in the host galaxy.

3.3. Neutral Carbon

Observationally the presence of a 2175 Å extinction feature is found to be correlated with the detection of neutral atomic carbon (Zafar et al. 2012; Ledoux et al. 2015; Ma et al. 2018) and/or molecules. This is consistent with a link between carbonaceous grain growth and the extinction bump (Henning & Salama 1998). For a sample of quasar absorbers, Ledoux et al. (2015) found that ~30% of the C I absorbers show a 2175 Å bump. Recently, Ma et al. (2018) found that all quasar absorbers with C I column densities above ~10^{14} cm^{-2} show a detectable bump feature in their SEDs. Based on a small sample, Zafar et al. (2012) reported a trend between C I equivalent widths and bump strengths. In the afterglow

spectrum of GRB 180325A, we detect strong C I absorption lines with restframe equivalent widths of $W_{\mathrm{r}}(\lambda 1560) = 0.58 \pm 0.05$ and $W_{\mathrm{r}}(\lambda 1656) = 0.85 \pm 0.05$. Comparing $W_{\mathrm{r}}(\mathrm{C\,I})$ and the area of the bump ($A_{\mathrm{bump}} = \pi\, c_3/2\gamma$; at the 1.6314 hr epoch it is 3.95 ± 0.20), the present burst follows the trend presented in Ma et al. (2018).

3.4. Host Galaxy Properties

In the VLT/X-shooter NIR spectrum, we clearly detect Hα and [O III] emission lines from the GRB host galaxy. We measure line fluxes of $F_{\mathrm{H}\alpha} = (5.0 \pm 1.2) \times 10^{-17}$ erg s^{-2} cm^{-1} Å^{-1} and $F_{[\mathrm{O\,III}]} = (7.7 \pm 0.9) \times 10^{-17}$ erg s^{-2} cm^{-1} Å^{-1} for these bright emission lines. The Hα line flux corresponds to a star formation rate (SFR) of $15.8 \pm 3.8\, M_\odot$ yr^{-1}, based on the calibration from Kennicutt (1998), and without correcting for dust extinction. Correcting for SED-derived dust extinction ($A_V \sim 1.5$), the host galaxy SFR is $46 \pm 4\, M_\odot$ yr^{-1}. We measure an FWHM of 106 ± 28 km s^{-1} for the Hα line. Using the correlation between stellar mass and velocity width of the Hα line derived for GRB host galaxies in Arabsalmani et al. (2018), we estimate a stellar mass of $M_*/M_\odot \sim 10^{9.3 \pm 0.4}$ for the host galaxy of GRB 180325A. The estimated stellar mass and SFR place the host galaxy among the main-sequence star-forming galaxies with similar redshifts, though toward higher SFRs on the envelope of the main-sequence SFR–M_* relation (see Figure 1 of Rodighiero et al. 2011). A larger specific SFRs (SFR per unit mass) than average is shown to be typical of GRB host galaxies (see Arabsalmani et al. 2018, and references therein).
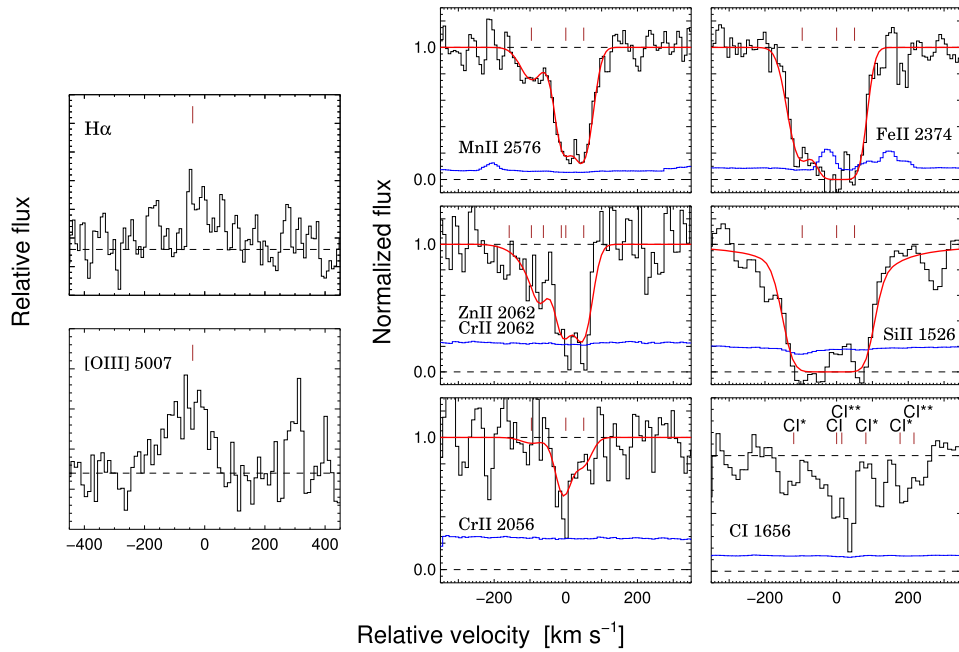
Figure 3. Left column: host galaxy Hα and [O III] emission lines. The central redshift of the GRB ($z = 2.2486$) is marked with vertical brown lines. Middle and right columns: normalized absorption-line profiles on a velocity scale centered at $z = 2.2486$. The spectra are shown as black curves with corresponding error spectra in blue. Voigt-profile fits are shown in red and top vertical brown lines represent different velocity components.

Table 3
GRB 180325A Metallicity with Respect to Solar

Elemental Transition	Component 1 $\log N_M$ (cm^{-2}) $b = 37.53 \pm 2.9$ km s^{-1}	Component 2 $\log N_M$ (cm^{-2}) $b = 20.9 \pm 5.5$ km s^{-1}	Component 3 $\log N_M$ (cm^{-2}) $b = 24.5 \pm 2.7$	Total $\log N_M$ (cm^{-2}) ⋯	Metallicity [M/H]
H I	⋯	⋯	⋯	22.30 ± 0.14	⋯
Fe II	14.87 ± 0.07	16.65 ± 0.18:	15.31 ± 0.23	16.68 ± 0.18:	> -1.35:
Mn II	12.94 ± 0.06	13.56 ± 0.08	13.73 ± 0.08	13.99 ± 0.08	> -1.90
Zn II	13.13 ± 0.14	13.66 ± 0.17	13.81 ± 0.15	14.09 ± 0.15	> -0.98
Si II	14.97 ± 0.37	15.18 ± 0.28	16.03 ± 0.52:	16.12 ± 0.48:	> -2.19:
Cr II	12.79 ± 1.13	13.75 ± 0.18	13.39 ± 0.37	13.94 ± 0.30	-2.00 ± 0.33

Note. The system has a three-component profile.

4. Discussion

We compared R_V, A_V, area of the bump (A_{bump}), and maximum height ($E_{\mathrm{bump}} = c_3/\gamma^2$) of GRB 180325A with other unambiguously detected GRB cases (GRB 070802 and GRB 080607: Zafar et al. 2011, GRB 080605 and GRB 080805: Zafar et al. 2012). Based on the 1.6314 hr SED results, we find this burst has wider bump area ($A_{\mathrm{bump}} = 3.95 \pm 0.20$), height ($E_{\mathrm{bump}} = 2.17 \pm 0.20$), and R_V than all known GRB cases but has a lower dust content when compared to GRB 080607 ($A_V = 2.33^{+0.46}_{-0.43}$; Zafar et al. 2011). However, the GRB 180325A bump area and height are still not as prominent as the mean MW ($A_{\mathrm{bump}}^{\mathrm{MW}} = 4.74$ and $E_{\mathrm{bump}}^{\mathrm{MW}} = 3.04$; Fitzpatrick & Massa 2007) and LMC average ($A_{\mathrm{bump}}^{\mathrm{LMC}} = 4.57 \pm 0.24$ and $E_{\mathrm{bump}}^{\mathrm{LMC}} = 3.12 \pm 0.17$; Gordon et al. 2003) bump. The extinction curve of GRB 180325A appears to be shallower than the mean MW (Fitzpatrick & Massa 2007) and average LMC (Gordon et al. 2003) curves.

Diffuse interstellar bands (DIBs) are a ubiquitous phenomenon in Galactic sightlines, and have been detected in a limited number of extragalactic sightlines (Magellanic Clouds, supernovae, quasar absorbers). Remarkably, the one SMC sightline that exhibits normal-strength DIBs includes a 2175 Å feature (Cox et al. 2007). The DIB carriers likely are large carbon-bearing molecules; C_{60}^+ has been proposed as the carrier of two (out of about 400) DIBs at 9577 and 9632 Å (Campbell et al. 2015). The measured (anomalous) extinction in GRB 180325A, and the presence of the 2175 Å feature, motivates the search for the presence of the strongest DIBs in its VLT/X-shooter spectrum. Several of them happen to be redshifted into the opaque regions in between the NIR windows, therefore, we cannot find a significant detection.

The presence of CO and H_2 molecules is usually correlated with the UV bump (e.g., Prochaska et al. 2009; Ledoux et al. 2015). The spectrum blueward of Lyα is strongly suppressed and due to low signal-to-noise around the blue end of spectrum, there is no clear detection of H_2 molecules. Neutral chlorine could also be used as a tracer of H_2 (Balashev et al. 2015). The afterglow spectrum of GRB 180325A has

relatively low signal-to-noise in the Cl I (λ1347 Å) region. The derived 3σ limit of $\log N(\text{Cl I/cm}^{-2}) < 14.20$ suggests $\log N(\text{H}_2/\text{cm}^{-2}) < 20.60$ based of correlation presented in Balashev et al. (2015). We also find no convincing detection of CO molecular lines because of low signal-to-noise and also partly because the spectral regions are blended with the strong intervening system at $z = 2.04$.

5. Conclusions

We here report the detection of a 2175 Å extinction bump in the spectrum of GRB 180325A afterglow at $z = 2.2486$, the only unambiguous detection over the past decade. For the first time, the extinction bump was spectroscopically observed at four different epochs, twice with the NOT/AlFOSC and twice with the VLT/X-shooter. We constructed the X-ray lightcurve from *Swift*-XRT and optical/NIR photometric lightcurves from GROND, NOT, and VLT/X-shooter. Using these multiband data, we generated SEDs at all four spectroscopic epochs. The SEDs fit well with a single power law and a 2175 Å extinction bump with $R_V \approx 4.4$, $A_V \approx 1.5$. The bump and extinction curve of GRB 180325A are shallower than the mean MW and LMC law. The derived metallicity of GRB is $[\text{Zn/H}] > -0.98$. The VLT/X-shooter spectrum exhibits neutral carbon at the GRB redshift, suggesting that strong C I is required to yield a 2175 Å bump. The dust-corrected SFR from the Hα emission-line flux is $\sim 46 \pm 4$ $M_\odot\,\text{yr}^{-1}$ and the predicted stellar mass is $\log M_*/M_\odot \sim 9.3 \pm 0.4$, which is representative for long-duration GRB hosts.

ORCID iDs

T. Zafar https://orcid.org/0000-0003-3935-7018
J. P. U. Fynbo https://orcid.org/0000-0002-8149-8298
D. Malesani https://orcid.org/0000-0002-7517-326X
J. Selsing https://orcid.org/0000-0001-9058-3892
D. A. Kann https://orcid.org/0000-0003-2902-3583
L. Christensen https://orcid.org/0000-0001-8415-7547
P. Møller https://orcid.org/0000-0002-9994-505X
D. Perley https://orcid.org/0000-0001-8472-1996
N. R. Tanvir https://orcid.org/0000-0003-3274-6336
D. H. Hartmann https://orcid.org/0000-0002-8028-0991
J. Hjorth https://orcid.org/0000-0002-4571-2306
S. Covino https://orcid.org/0000-0001-9078-5507
L. Izzo https://orcid.org/0000-0001-9695-8472
R. Salvaterra https://orcid.org/0000-0002-9393-8078

References

Arabsalmani, M., Møller, P., Fynbo, J. P. U., et al. 2015, MNRAS, 446, 990
Arabsalmani, M., Møller, P., Perley, D. A., et al. 2018, MNRAS, 473, 3312
Arnaud, K. A. 1996, in ASP Conf. Ser. 101, Astronomical Data Analysis Software and Systems V, ed. G. H. Jacoby & J. Barnes (San Francisco, CA: ASP), 17
Asplund, M., Grevesse, N., Sauval, A. J., & Scott, P. 2009, ARA&A, 47, 481
Balashev, S. A., Noterdaeme, P., Klimenko, V. V., et al. 2015, A&A, 575, L8
Buat, V., Giovannoli, E., Heinis, S., et al. 2011, A&A, 533, A93
Campbell, E. K., Holz, M., Gerlich, D., & Maier, J. P. 2015, Natur, 523, 322
Cano, Z., Wang, S.-Q., Dai, Z.-G., & Wu, X.-F. 2017, AdAst, 2017, 8929054
Covino, S., Melandri, A., Salvaterra, R., et al. 2013, MNRAS, 432, 1231
Cox, N. L. J., Cordiner, M. A., Ehrenfreund, P., et al. 2007, A&A, 470, 941
Cucchiara, A., Fumagalli, M., Rafelski, M., et al. 2015, ApJ, 804, 51
Draine, B. T. 2003, ARA&A, 41, 241
Elíasdóttir, Á, Fynbo, J. P. U., Hjorth, J., et al. 2009, ApJ, 697, 1725
Evans, P. A., Beardmore, A. P., Page, K. L., et al. 2009, MNRAS, 397, 1177
Fitzpatrick, E. L. 2004, in ASP Conf. Ser. 309, Astrophysics of Dust, ed. A. N. Witt, G. C. Clayton, & B. T. Draine (San Francisco, CA: ASP), 33
Fitzpatrick, E. L., & Massa, D. 1990, ApJS, 72, 163
Fitzpatrick, E. L., & Massa, D. 2007, ApJ, 663, 320
Fynbo, J. P. U., Krühler, T., Leighly, K., et al. 2014, A&A, 572, A12
Fynbo, J. U., Holland, S., Andersen, M. I., et al. 2000, ApJL, 542, L89
Gordon, K. D., Clayton, G. C., Misselt, K. A., Landolt, A. U., & Wolff, M. J. 2003, ApJ, 594, 279
Heintz, K. E., Fynbo, J. P. U., Jakobsson, P., et al. 2017, A&A, 601, A83
Heintz, K. E., Fynbo, J. P. U., & Malesani, D. 2018, GRB Coordinates Network, Circular Service, No., 22535
Henning, T., & Salama, F. 1998, Sci, 282, 2204
Jiang, P., Ge, J., Zhou, H., Wang, J., & Wang, T. 2011, ApJ, 732, 110
Kennicutt, R. C., Jr. 1998, ARA&A, 36, 189
Kriek, M., & Conroy, C. 2013, ApJL, 775, L16
Krogager, J.-K. 2018, arXiv:1803.01187
Krühler, T., Küpcü Yoldaş, A., Greiner, J., et al. 2008, ApJ, 685, 376
Ledoux, C., Noterdaeme, P., Petitjean, P., & Srianand, R. 2015, A&A, 580, A8
Ma, J., Ge, J., Prochaska, J. X., et al. 2018, MNRAS, 474, 4870
Maíz Apellániz, J., & Rubio, M. 2012, A&A, 541, A54
Mathis, J. S. 1994, ApJ, 422, 176
Mattsson, L., Wahlin, R., Höfner, S., & Eriksson, K. 2008, A&A, 484, L5
Noll, S., Pierini, D., Pannella, M., & Savaglio, S. 2007, A&A, 472, 455
Perley, D. A., Morgan, A. N., Updike, A., et al. 2011, AJ, 141, 36
Prochaska, J. X., Sheffer, Y., Perley, D. A., et al. 2009, ApJL, 691, L27
Reddy, N. A., Oesch, P. A., Bouwens, R. J., et al. 2018, ApJ, 853, 56
Rodighiero, G., Daddi, E., Baronchelli, I., et al. 2011, ApJL, 739, L40
Sari, R., Piran, T., & Narayan, R. 1998, ApJL, 497, L17
Schlafly, E. F., & Finkbeiner, D. P. 2011, ApJ, 737, 103
Scoville, N., Faisst, A., Capak, P., et al. 2015, ApJ, 800, 108
Selsing, J., Malesani, D., Goldoni, P., et al. 2018, arXiv:1802.07727
Starling, R. L. C., Wiersema, K., Levan, A. J., et al. 2011, MNRAS, 411, 2792
Stecher, T. P. 1965, ApJ, 142, 1683
Vernet, J., Dekker, H., D'Odorico, S., et al. 2011, A&A, 536, A105
Willingale, R., Starling, R. L. C., Beardmore, A. P., Tanvir, N. R., & O'Brien, P. T. 2013, MNRAS, 431, 394
Zafar, T., Watson, D., Elíasdóttir, Á, et al. 2012, ApJ, 753, 82
Zafar, T., Watson, D., Fynbo, J. P. U., et al. 2011, A&A, 532, A143
Zafar, T., Watson, D., Møller, P., et al. 2018, arXiv:1805.07016
Zeimann, G. R., Ciardullo, R., Gronwall, C., et al. 2015, ApJ, 814, 162